11th World Congress on Computational Mechanics (WCCM XI)
5th European Conference on Computational Mechanics (ECCM V)
6th European Conference on Computational Fluid Dynamics (ECFD VI)
E. Oñate, J. Oliver and A. Huerta (Eds)

ADJOINT OPTIMIZATION OF A COOLANT PUMP IMPELLER

Sabine Baumbach*

* Volkswagen AG, Component Development HME
Letter box 7359, D-38231 Salzgitter, Germany
e-mail: sabine.baumbach@volkswagen.de

Key words: adjoint approach, shape optimization, morphing, centrifugal pumps, industrial applications

Abstract. While the adjoint method is already in use for external aerodynamics and internal duct optimization in automotive industry [1, 2, 3, 4], the application range is by far not exhausted. Based on the available continuous adjoint implementation at Volkswagen [1], the framework is extended to rotating engine components. In the present work the adjoint method is applied to an engine coolant pump to increase the hydraulic efficiency by adapting the impeller shape. It is investigated how the sensitivity map can be tranferred into a shape update. The available mesh motion tools in OpenFOAM®, as well as morphing with the commerical tool ANSA® are analysed.

1 INTRODUCTION

While bionic optimization procedures such as evolutionary strategies and genetic algorithms are already well established in automotive industry, the adjoint approach has also considerably gained in importance. Although bionic optimizations are known for their robustness and stability, computations with high amounts of design parameters tend to increase the computation time drastically. Where bionic optimizations are not feasible the adjoint approach is a welcomed alternative. Independent of the number of design variables the cost to determine the gradient is comparable to solving two flow equations, because the adjoint and the primal equation system are of equal complexity [5].

The adjoint framework has been mostly used in external aerodynamics [5, 6], automotive industry recognised the potential of the gradient based optimization method as well and started adapting the method to their specific needs, thus the method matured over time and is now the first choice for gradient based optimizations. Othmer [1] extended the formulation of the previous adjoint approaches to fit the needs of automotive industry. Several examples such as the optimization of the external car body, air ducts for cabin ventilation and engine intake ports show the huge potential of the method [1, 2, 3, 4].

This work contributes by investigating how to apply the previous framework to rotating engine components namely coolant pumps.

Although the basic adjoint framework for rotating components is already well known [6, 7, 8, 9], less work has been done so far on how to interpret and actually set up an adjoint optimization process for rotating engine components in industry. This work proposes a shape optimization process for a coolant pump impeller using the open source software OpenFOAM®. To reduce computational cost steady state simulations applying multi reference frames (MRF) are conducted. The aim of the work is to identify the optimal impeller geometry while maximizing the hydraulic efficiency. Thus the mesh motion tools available in OpenFOAM® , as well as morphing with the commercial tool ANSA® are investigated. The limits and capabilities of the mesh motion features in OpenFOAM® with regards to shape optimization are outlined and compared to the capabilities offered by commercial tools. The aim of this work is to set up an automatic optimization loop for improving the design of incompressible fluid flow impellers and thus show the potential of the proposed method.

2 GOVERNING EQUATIONS

Two different adjoint approaches have been developed in the past, namely the discrete and continuous adjoint. Due to the already developed adjoint framework in OpenFOAM® and the additional solver packages customized to the needs of automotive industry available at Volkswagen the continuous adjoint approach is pursued here and thus the derivations are shown for the continuous approach.

The aim of the adjoint method is to compute the gradient of the cost function J subject to the flow variables, velocity $\vec{v}$ and pressure p, and the design variable $\vec{\beta}$. As introduced by Pironneau [10] the design variable $\vec{\beta}$ is defined as surface displacement in normal direction. The optimization problem therefore is given by

$$\text{maximize } J = J(\vec{v}, p, \vec{\beta}) \text{ subject to } \mathbf{R}(\vec{v}, p) = 0, \tag{1}$$

where $\mathbf{R} = (R_1, R_2, R_3, R_4)$ are the 3 dimensional steady state Navier-Stokes (NS) equations. In general time accurate simulations are required to compute the flow in centrifugal pumps and thus capture the unsteady flow field [11]. Here an intermediate approach is pursued to save resources. A reference frame is applied and the rotational forces emerge as additonal source terms in the NS equation.

$$\begin{aligned} (R_1, R_2, R_3)^T &= (\vec{w} \cdot \nabla)\vec{v} + \nabla p - \nabla \cdot (2\nu \mathbf{D}(\vec{v})) + (\vec{\omega} \times \vec{v}), \\ R_4 &= -\nabla \cdot \vec{v}, \end{aligned} \tag{2}$$

where $\vec{\omega}$ is the rotational velocity, $\vec{w}$ the relative velocity, ν the kinematic viscosity and $\mathbf{D}$ the rate of strain given as $\mathbf{D} = \frac{1}{2}(\nabla\vec{v} + (\nabla\vec{v})^T)$. To take the turbulence model of the primal solver into account the kinematic viscosity is the sum of molecular and turbulent viscosity. Instead of deriving an adjoint analogue to turbulence, in the current work

the frozen turbulence approach is used, so no additional adjoint equations for turbulent variables are solved.

The variation of the cost function and the state equations with respect to the flow field and design variables are given by

$$\begin{aligned} \delta J &= \frac{\partial J}{\partial \vec{v}}\delta\vec{v} + \frac{\partial J}{\partial p}\delta p + \frac{\partial J}{\partial \vec{\beta}}\delta\vec{\beta}, \\ \delta R &= \frac{\partial R}{\partial \vec{v}}\delta\vec{v} + \frac{\partial R}{\partial p}\delta p. \end{aligned} \tag{3}$$

Considering we have a constrained optimization problem where the state equations are the constraint, the optimization problem can be rephrased by using Lagrange multipliers and thus introducing the adjoint flow variables $\psi = (\vec{u}, q)$: velocity $\vec{u}$ and pressure q

$$L = J - \int_\Omega \psi \ \mathbf{R} \ \mathrm{d}\Omega. \tag{4}$$

To compute the sensitivities with respect to the design variables, the total variation of the Lagrange function is evaluated

$$\delta L := \delta_{\vec{\beta}} L + \delta_{\vec{v}} L + \delta_p L. \tag{5}$$

The Lagrangian multipliers are choosen so that the variation with respect to the flow variables vanish

$$\delta_{\vec{v}} L + \delta_p L := 0. \tag{6}$$

Now the gradient of the cost function with respect to the design variable can be computed

$$\delta_{\vec{\beta}} L = \delta_{\vec{\beta}} J - \int_\Omega \psi \ \delta_{\vec{\beta}} \mathbf{R} \ \mathrm{d}\Omega. \tag{7}$$

Equation (6) is used to determine the adjoint flow system and adjoint boundary conditions. After the primal and adjoint flow system are solved, equation (4) can easily be used to evaluate the surface sensitivities.

3 COST FUNCTION AND BOUNDARY CONDITIONS

To improve the performance of the pump the hydraulic efficiency shall be increased by adapting the design of the impeller. In order to compute the hydraulic efficiency of the waterpump the pressure difference between inlet and outlet as well as the mechanical work at the impeller are considered. The energy required to accelerate the fluid can be computed over the moment at the impeller. Thus the cost functions of interest are as follows

- pressure

$$\int_{\Gamma_{\text{Inlet}}} \left(p + \frac{1}{2}\rho v^2 \right) \mathrm{d}\Gamma_{\text{Inlet}} - \int_{\Gamma_{\text{Outlet}}} \left(p + \frac{1}{2}\rho v^2 \right) \mathrm{d}\Gamma_{\text{Outlet}}, \tag{8}$$

- moment at impeller

$$\int_{\Gamma_{\text{Impeller}}} \left(p\mathrm{d}\vec{A} + \tau \cdot \mathrm{d}\vec{A} \right) \cdot (\vec{\omega} \times \vec{r}) \; \mathrm{d}\Gamma_{\text{Impeller}}. \tag{9}$$

In equation (9) p refers to the pressure at the surface, τ is the wall shear stress, $\vec{A}$ is the surface vector, $\vec{\omega}$ is the rotational velocity and $\vec{r}$ is the local vector of the surface element.

Both cost functions are combined by weighting factors

$$J = \frac{\sum\limits_{i_\Gamma} \alpha_i \; \mathrm{J}_i}{\sum\limits_{i_\Gamma} \alpha_i}, \tag{10}$$

for a multiobjective optimization.

To compute the primal flow field no-slip velocity conditions are applied at all stationary walls and the velocity at the inlet and the impeller is fixed at its described value $\vec{v_0}$. Moreover, a zero pressure gradient holds true at the inlet and the impeller. At the outlet a constant pressure is applied and a zero velocity gradient assumed. Thus the primal boundary conditions are given as

- Primal boundary conditions for Wall/Inlet/Impeller

$$\vec{v} = \begin{cases} 0 \text{ , at Wall,} \\ \vec{v_0} \text{ , at Inlet/Impeller,} \end{cases} \tag{11}$$

$$\nabla p = 0, \tag{12}$$

- Primal boundary conditions for Outlet

$$\nabla \vec{v} = 0, \tag{13}$$

$$p = p_0. \tag{14}$$

Now following the derivation by Othmer [1] the adjoint boundary conditions result

- Adjoint boundary conditions for Wall/Inlet/Impeller

$$\vec{u_t} = 0, \tag{15}$$

$$u_n = \begin{cases} 0 \text{ , at Wall} \\ -\frac{\delta J_\Gamma}{\delta p} \text{ , at Inlet/Impeller,} \end{cases} \tag{16}$$

$$\vec{n} \cdot \nabla q = 0, \tag{17}$$

- Adjoint boundary conditions for Outlet

$$q = \vec{u} \cdot \vec{v} + u_n v_n + \nu(\vec{n} \cdot \nabla) u_n + \frac{\delta J_\Gamma}{\delta v_n}, \tag{18}$$

$$0 = v_n \vec{u_t} + \nu(\vec{n} \cdot \nabla) \vec{u_t} + \frac{\delta J_\Gamma}{\delta \vec{v_t}}. \tag{19}$$

In the boundary conditions contributions of the cost functions appear. Considering that the cost function *pressure* is only defined between the inlet and the outlet, the inlet condition is fulfilled with $u_n = v_0$ and the outlet boundary condition yields $q = \vec{u} \cdot \vec{v} + u_n v_n + \nu(\vec{n} \cdot \nabla) u_n - 0.5 v^2 - v_n^2$. At the impeller a constant adjoint velocity $\vec{u} = \vec{\omega} \times \vec{r}$ is applied.

4 OPTIMIZATION PROCEDURE

The continuous adjoint framework is implemented into an automatic optimization procedure where the impeller shape is changed in accordance with the sensitivities. Several issues are encountered when the surface sensitivities are used to set the mesh motion.

To avoid high mesh deformations the displacement of the surface elements should be in orders of magnitude of the elements size thus the sensitivities are scaled before mesh motion. Moreover, the sensitivities are scalar values, so to get the displacement the sensitivity field is multiplied with the surface normal vectors. Each element of the impeller surface is thus displaced with regards to the calculated sensitivity. The motion at all other boundaries is set to zero. To solve for the deformation of the volume mesh an additional equation is solved where the surface displacements are used as boundary conditions. Although the displacements in the mesh are rather small, depending on the mesh motion equation with advancing mesh motion steps severe mesh degradation effects generally occur. One reason for this phenomenon to occur is the ragged sensitivity field at the boundaries. Large sensitivity deviations between neighboring elements result in high nonlinear deformations and thus an early termination of the optimization run.

Moreover, the sensitivities at the single blades depend on the relative position of the blade to the pump discharge. It is clear that the blade positioned closest by the discharge exhibits higher magnitudes of shear stress than the other blades and thus the highest sensitivities are likely to occur here. So if the surfaces of the blades are displaced according to the sensitivity map at the blade, different blade shapes result leading to imbalance and uneven rotation of the pump. So before moving the mesh the sensitivities are averaged over all blades in an additional postprocessing step.

In this work two different approaches to solve the encountered problems are pursued. The mesh morphing capabilities of ANSA®, as well as the OpenFOAM® own mesh motion tools are tested and compared to each other. First the primal and adjoint flow fields are computed. Afterwards the sensitivities at the impeller are calculated using

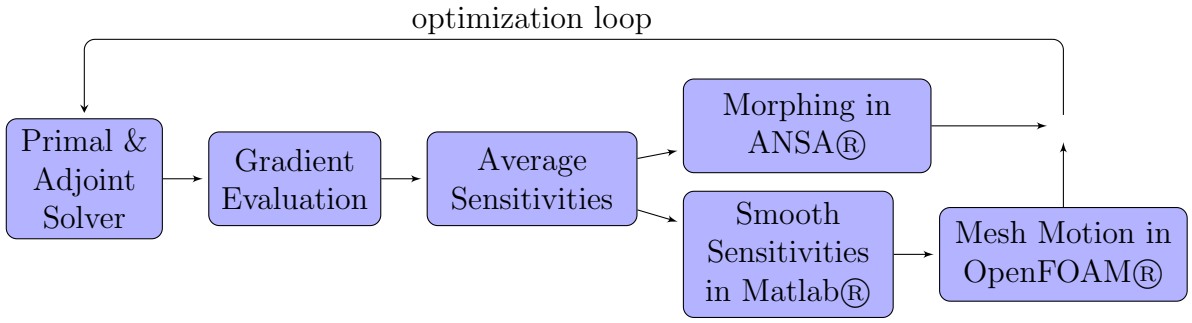

Figure 1: Optimization loop

the primal and adjoint flow variables. To preserve a symmetric impeller an additional postprocessing routine in Matlab® is called which averages and smoothes the sensitivities over all blades. The new sensitivities are used as input in OpenFOAM® and ANSA® to morph the mesh. The topology is not changed thus the optimization run can easily be started again until a satisfactory result is obtained. The whole optimization cycle is shown in figure (1).

ANSA® offers the capability to read in sensitivities calculated in OpenFOAM® and morph a mesh directly with respect to the sensivity values at the boundary. The advantage of using ANSA® are the easy set up and the high deformations of the mesh while the mesh quality does not degrade. Unfortunately, this feature is not yet available for scripting thus the user has to manually interfere in the optimization run and morph the mesh manually. Therefore it is also analysed whether the available mesh motion tools in OpenFOAM® can be adapted to set up a well working optimization cycle.

5 TEST CASE

Two different cases are set up to test the suggested optimization cycles. A quasi three dimensional (3d) and a 3d case are investigated. The quasi 3d case is the meridional surface within the water pump. The surface is extended by one cell in plane normal direction and symmetry boundary conditions are applied at the top and bottom of the computational mesh. Although the case does not represent the 3 dimensional complex flow within the pump, it reaches convergence fast and thus is suitable to study the behaviour of the optimization process and conduct a parameter study.

The 3d case is more complex. The geometry of the pump is shown in figure (2). The fluid enters at the top of the impeller, is accelerated by the rotating impeller and than leaves after flowing through the volute casing. The arrows in figure (2) show the direction of the flow. The impeller consists of five blades.

The meshes of both cases are unstructured and created in ANSA®. The quasi 3d mesh contains 1,013,586 nodes and 600,372 cells, while the 3d mesh contains 3,856,809 nodes and 9,404,262 cells. The primal solver uses turbulent wall functions, the adjoint

solver contains no wall functions, therefore both cases are meshed with boundary layers to resolve the near-wall flow.

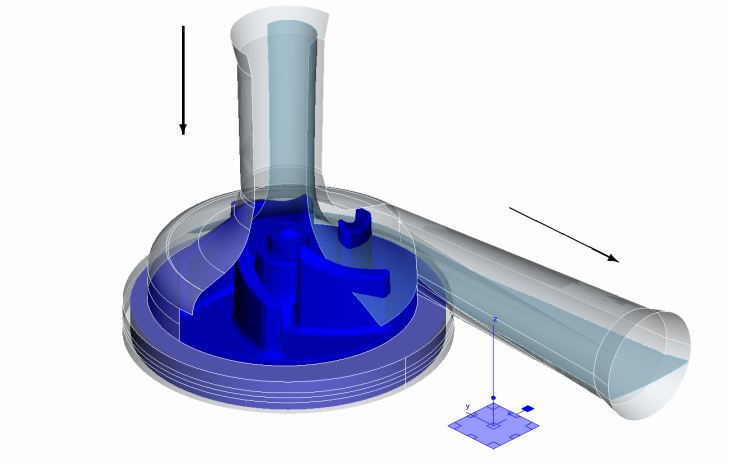

Figure 2: Cut through the waterpump showing the impeller and the volute casing. The light blue surface shows the quasi 3d computation domain. Rotating parts are colored in dark blue. Please note that the pump is cut in z direction. The arrows show the flow direction.

The primal solution is computed using the SIMPLE method and the k-ω-SST turbulence model is applied.

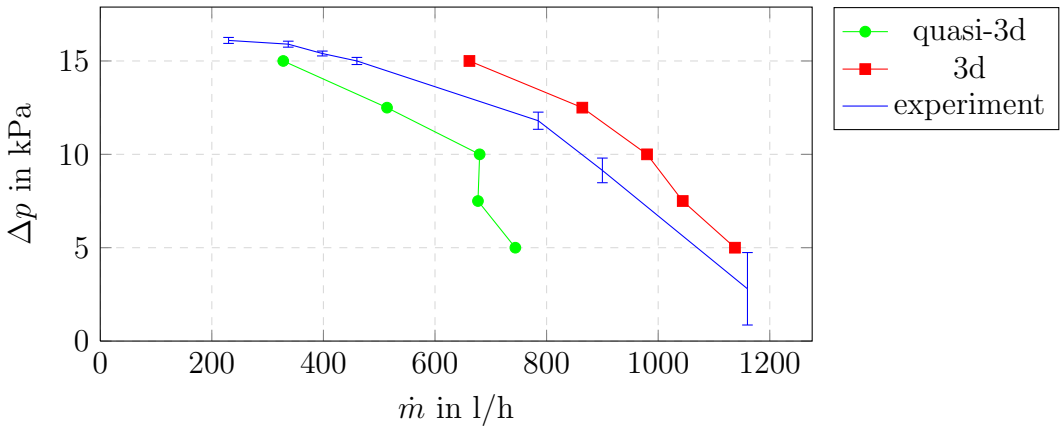

Figure 3: Pressure difference Δp as function of mass flow $\dot{m}$ at $n = 3000\ U/min$: comparison of quasi-3d, 3d computations and experiment. The quasi 3d computations are scaled in accordance to the mass flow.

Before starting the optimization procedure and adapting the impeller shape it is investigated how well the simulations agree with experimental results. Figure (3) shows the pressure difference $\triangle p$ between inlet and outlet as a function over the massflow $\dot{m}$ at a constant rotational speed $n = 3000$ U/min. A good agreement between 3d computations

and experiments is achieved. The high deviations between quasi 3d computations and experiments are due to the reduction of the complex 3d geometry to a single surface. Losses due to the gap between impeller and volute casing, the flow separation at the nozzle and the flow around the lower part of the rotor are not regarded, so with smaller mass flows higher pressures are reached. With increasing massflow the deviations between experimental values and simulation results become more important. It is observed that the quasi 3d computations with increasing massflow no longer converge. Nevertheless, good agreement at the design point (massflow of $\dot{m} = 500$ l/min at a rotational speed of $n = 3000$ U/min) is reached. This setup is also used for the adjoint computations.

6 RESULTS

6.1 QUASI 3D CASE

In Figure (4) the increase in hydraulic efficiency η is plotted over the number of mesh motion steps for OpenFOAM® and ANSA® . Four different smoothing parameters are applied while using OpenFOAM own mesh motion tools. The smallest smoothing is labeled with p_1 and the highest smoothing is applied in case p_4. So with higher smoothing more neighbors are taken into account to flatten the surface sensitivitities. A steady increase in efficiency is visible for each optimization run independent on the smoothing and mesh motion tool. In OpenFOAM® the best result is yielded using the mesh smoothing p_3. An overall gain of 9.2 % efficiency after 53 mesh motion steps is recorded. While in ANSA® the efficiency increases to 21.8 % after 12 mesh motion steps.

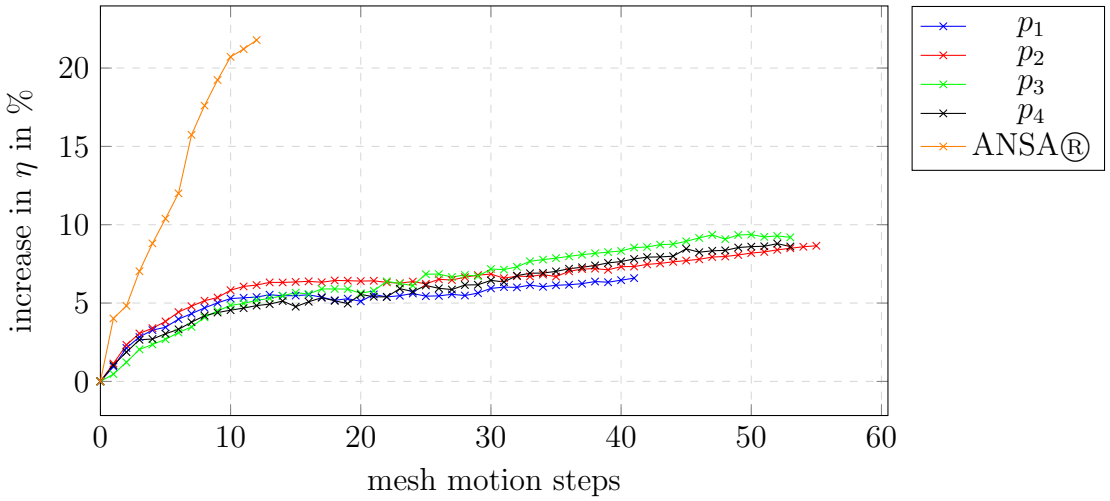

Figure 4: The increase in hydraulic efficiency of the quasi 3D cases is plotted over the mesh motion. The first four plots show the computations in OpenFOAM® for different sensitivity smoothing parameters. The last plot shows the efficiency increase obtained by using ANSA® for mesh motion.

Using the mesh motion tools of OpenFOAM® a slow degradation of the mesh quality

occurs. After about 50 mesh motion steps dependent on the applied smoothing the mesh quality has reduced so far that continuing the optimization run would no longer obtain reasonable results, so the optimization process is terminated. It is observed that with less smoothing, the mesh quality degenerates faster. Especially problematic for OpenFOAM® is the preservation of the boundary layers. Neither the layer thickness nor the quality is preserved while transforming the mesh. Nevertheless, the same trends in shape design are visible independent of the mesh motion tool.

6.2 3D CASE

Two optimization cycles for the 3d case are run, one cycle using the OpenFOAM® own mesh motion tools and the other cycle using ANSA® . Starting from the converged primal and adjoint fields the optimization cycle runs for 12 steps in ANSA® and 35 steps in OpenFOAM®. The averaged and smoothed sensitivity map at the start of the optimization cycle is shown in figure (5).

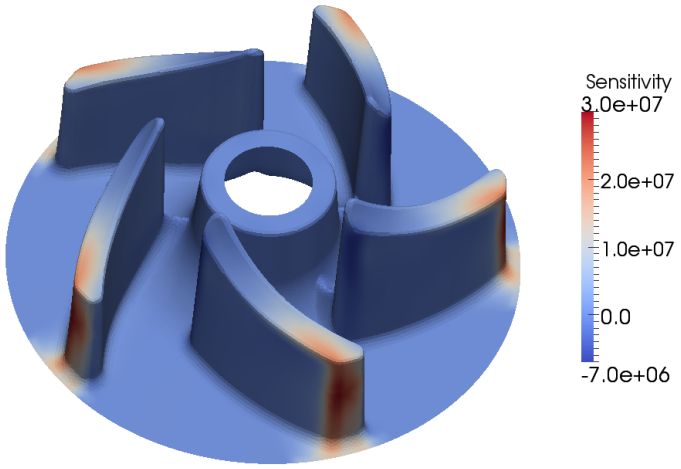

Figure 5: Sensitivities at the impeller. Blue zones (negative sensitivity values) refer to motion into the fluid domain, red zones (positive sensitivity values) refer to motion out of the fluid domain.

The results of the optimization cycle for the 3d case are plotted in figure (6). The increase in efficiency η, as well as the increase in input and output power are plotted over the mesh motion steps. A steady increase in η of 7.2 % in ANSA® and 1.5 % in OpenFOAM® is seen. In OpenFOAM®the displacement in each mesh motion step is smaller than in ANSA®. To preserve the mesh quality in OpenFOAM®more mesh motion steps are needed to reach an efficiency increase comparable to the one accomplished with mesh motion in ANSA®. While the output power stays constant, the input power decreases. So with the chosen weighting of the cost functions the losses at the impeller have been reduced and less input power is necessary to reach the same output.

The original blade and the final blade shapes in the meridional plane are plotted in

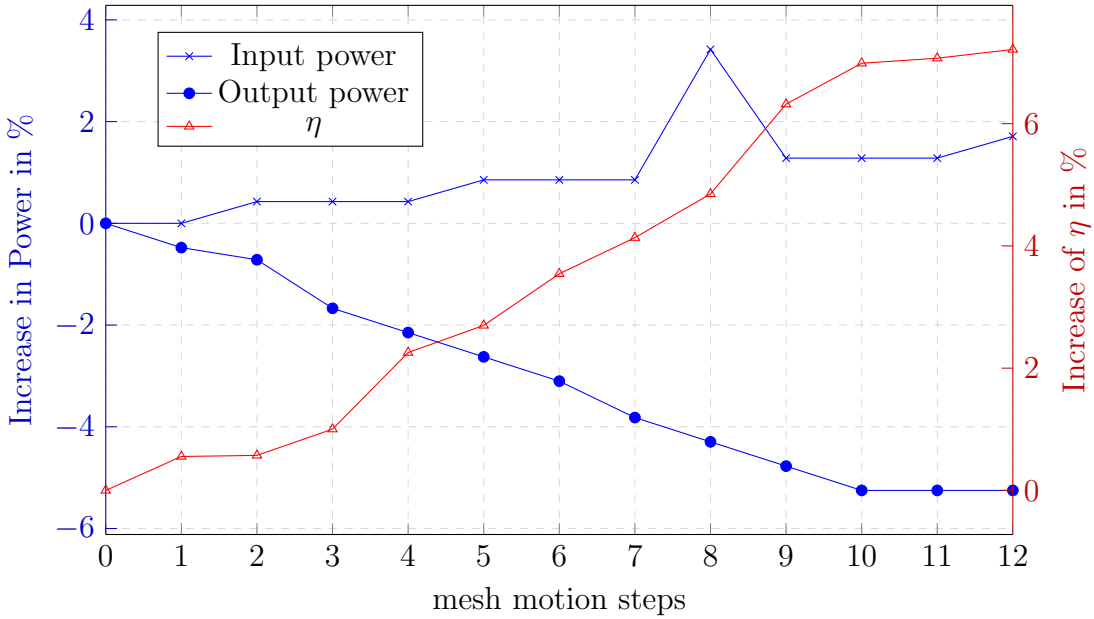

Figure 6: Increase in Input, Output power and hydraulic efficiency plotted over mesh motion steps for optimization cycles in ANSA®.

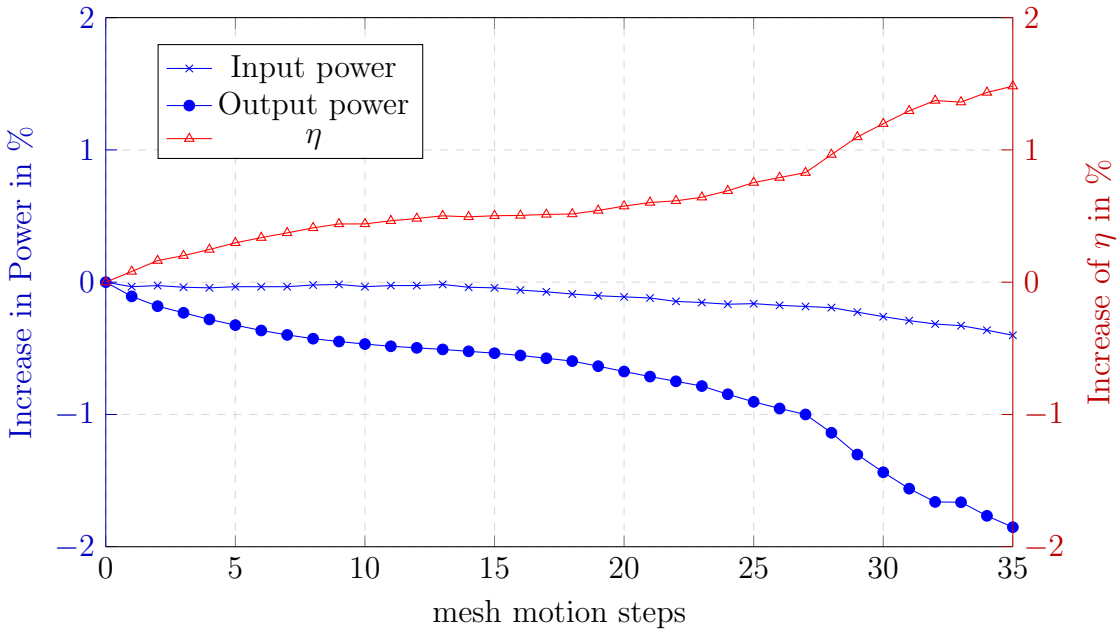

Figure 7: Input, Output power and hydraulic efficiency plotted over mesh motion steps for optimization cycles in OpenFOAM®.

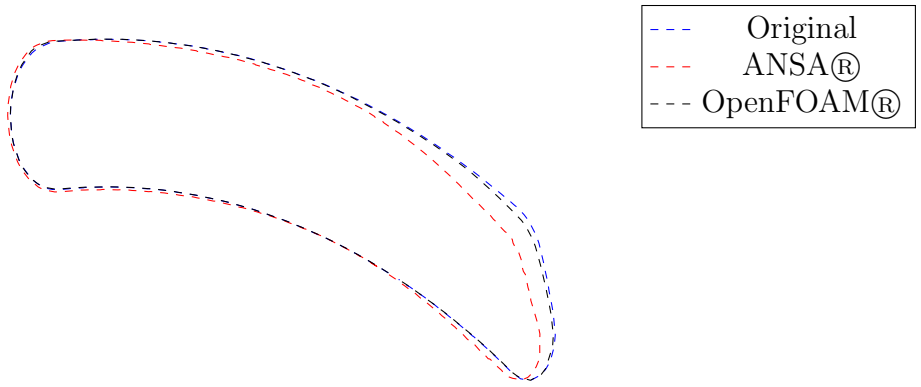

Figure 8: Meridional cut through impeller showing the original and final blade designs.

figure (8). According to the sensitivities shown in figure (5) the efficiency is improved by flattening the trailing edge and extruding the leading edge. While just slight changes at the leading edge are visible, the trailing edge has noticeably been transformed. The blade becomes thinner and the radius at the trailing edge is increased.

7 CONCLUSION

- The primal and adjoint equation systems are solved in OpenFOAM® and a post-processing step is introduced to average and smooth the sensitivities.

- To adapt the impeller shape with respect to the sensitivities two different mesh motion tools are investigated with the aim to increase the hydraulic efficiency of a waterpump. While mesh motion in OpenFOAM® allows a fully automatic optimization process, it is not yet possible to run the optimization in ANSA® without a certain degree of manual user intervention.

- The results for a quasi 3d computation and a 3d computation are presented. A total increase of hydraulic efficiency of 21.8 % in the quasi 3d and 7.2 % in the 3d geometry are achieved. Nevertheless, steady state simulations are conducted where just one specific impeller position is taken into account. Therefore the actual gain in efficiency might differ.

8 ACKNOWLEDGEMENT

The author would like to thank Dr. Andreas Gitt-Gehrke and Dr. Carsten Othmer at Volkswagen for many helpful discussions related to the current work. The author also gratefully acknowledges the support of Prof. Dr.-Ing. Jens Friedrichs from the Institute of Jet Propulsion and Turbomachinery at Technical University Braunschweig. Finally, this work would not have been possible without the generous help of the component development at Volkswagen Salzgitter.

REFERENCES

[1] C. Othmer *A continuous adjoint formulation for the computation of topological and surface sensitivities of ducted flows*. International Journal for Numerical Methods in Fluids, 58(8):862-877, 2008.

[2] C. Othmer *Adjoint-based topology and shape optimization for automotive applications*. ERCOFTAC Design Optimization, 2013.

[3] C.Hinterberger and M.Olesen *Industrial application of continuous adjoint flow solvers for the optimisation of automotive exhaust systems*. ECCOMAS , 2011.

[4] E. Helgason and S.Krajnović *Aerodynamic shape optimization of a pipe using the adjoint method*. ASME 2012 International Mechanical Engineering Congress & Exposition, 9-15 November, 2012.

[5] A. Jameson *Aerodynamic Design via Control Theory* Journal of Scientific Computing, Vol. 3, No. 3, 1988

[6] D.I. Papadimitriou and K.C. Giannakoglou *Compressor blade optimization using a continuous adjoint formulation* ASME TURBO EXPO, GT2006/90466, 8-11 May, 2006.

[7] A.C. Marta, S. Shankaran, Q. Wang and P. Venugopal *Interpretation of adjoint solutions for turbomachinery flows*. AIAA Journal, 51(7):1733-1744, 2013.

[8] E. Nielsen, E. M. Lee-Rausch and W. T. Jones *Adjoint-Based Design of Rotors Using the Navier-Stokes Equations in a Noninertial Reference Frame* American Helicopter Society 65th Annual Forum, 27-29 May, 2009.

[9] T. D. Economon, F. Palacios and J. J. Alonso *A Viscous Continuous Adjoint Approach for the design of Rotating Engineering Applications* AIAA Paper, AIAA Computational Fluid Dynamics Conference, 24-27 June, 2013.

[10] O. Pironneau *Optimal shape design for elliptic systems* Springer, 1984.

[11] S. K. Nadarajah and A. Jameson *Optimum Shape Design for Unsteady Flows with Time-Accurate Continuous and Discrete Adjoint Methods* AIAA Journal, Vol. 45, No. 7, 2007

[12] S. Choi, M. Potsdam and K. Lee *Helicopter Rotor Design Using a Time-Spectral and Adjoint-Based Method* Multidisciplinary Analysis and Optimization Conference, 12th AIAA/ISSMO, 10-12 September, 2008.

[13] MATLAB Release 2013a, The MathWorks, Inc. Natick, Massachusetts, United States.

[14] OpenFOAM: *http://www.opencfd.co.uk/openfoam/index.html*